



Trapping waves with tunable prism-coupling terahertz metasurfaces absorber

YI HUANG,¹ SHUNCONG ZHONG,^{1,2,*}  TINGTING SHI,¹ YAO-CHUN SHEN,³  AND DAXIANG CUI⁴

¹Laboratory of Optics, Terahertz and Non-Destructive Testing, School of Mechanical Engineering and Automation, Fuzhou University, Fuzhou 350108, China

²Department of Precision Mechanical Engineering, School of Mechatronic Engineering and Automation, Shanghai University, 200072, China

³Department of Electrical Engineering and Electronics, University of Liverpool, L69 3BX, United Kingdom

⁴Department of Bio-Nano Science and Engineering, Shanghai Jiaotong University, 200030, China

*zhongshuncong@hotmail.com

Abstract: We experimentally demonstrated a corrugated metallic metasurface based tunable perfect absorber for terahertz (THz) frequencies in a total internal reflection geometry. The absorbance is strongly depend on the central layer of this three-layer absorber, which provides a feasible approach to tune the absorption. In particular, there exist an optimal gap that enables a perfect absorption at specific frequency. Due to the simple 1D geometric structure of metasurface, its absorption frequency can be easily tailored over a wide frequency range (0.625–1.499 THz). More importantly, the modulation of the effective refractive index and loss of medium environment can be accepted as an alternative approach for the absorption properties modulation. This prism coupling absorber provides a new route for modulation of the absorption characteristics with potential applications in biological sensing.

© 2019 Optical Society of America under the terms of the [OSA Open Access Publishing Agreement](#)

1. Introduction

In recent years, terahertz (THz, the so-called ‘terahertz gap’ between 0.1 THz and 10 THz) radiation as one of the most exciting research hotspot, has attracted much attention due to its wide potential applications in imaging [1], communication [2], astronomy [3], nondestructive inspection [4], particularly in biological and chemical sensing [5,6]. Because of the ability to control electromagnetic waves in a unique manner, metasurfaces (typically referring to spoof plasmon surfaces, SPS) decorated with periodic patterns, such as cylinders [7], V-shaped blocks [8], and split rings [9], have attracted great research interests, especially in metasurfaces perfect absorbers (MPAs). MPAs has become an important role in the realization of terahertz devices, including high-resolution terahertz detection [10], imaging [11], sensing [12], etc.

The first experimental observation of near unity absorption achieved by a metasurface perfect absorber with sandwich structure in the microwave regime were reported by Landy et al. [13] in 2008. Since then, extensive research have focused on the metasurfaces based perfect absorber with multilayer approaches which minimizing the reflectivity via matching the impedance to free-space and simultaneously suppressing the transmission via using a metallic ground plane. By modulating the shapes or sizes of unit cell of metasurfaces, the operating frequency bands of MPAs have been expanded from microwave to terahertz. Meanwhile, on the basis of the tailored response of metasurfaces, various terahertz metasurface absorbers with unique absorption characteristics, such as narrowband [14], broadband [15] or multiband absorption [16], and insensitivity to angle of incidence [17] and polarization [18], have been widely investigated and demonstrated. Nevertheless, most of the current reports mainly focused on the absorption strength modulation rather than the resonance frequency modulation [19]. Although various desirable absorption properties of MPAs in the THz regime have been explored by designing

complex geometric patterns, it is very difficult to conduct the resonance frequency modulation and achieve perfect absorption simultaneously, which greatly limits their practical applications. It is also worth noting that an abundant development of absorption behaviors occurs with varying dielectric layer thicknesses [20]. But, MPAs usually fabricated with a stationary dielectric layer thickness, limiting the tunability of the absorption [21].

In this letter, we design a single-frequency terahertz perfect absorber based on metallic metasurfaces decorated with periodic subwavelength trapezoidal grooves. Spoof surface plasmon resonances (SPR) induced on the designed metasurfaces with a polyethylene (PE) prism are considered as an alternative mechanism for the generation of electromagnetic wave absorption. We experimentally demonstrated the absorption response of the MPA to the tunable space layer gap and the depth of grooves. A perfect absorption can be acquired when the space layer reaches the optimal value. Moreover, the resonance frequency can be tune to the lower frequency region by increasing the depth of grooves. Finally, we also demonstrate that the modulation of absorption properties by changing the refractive index and loss inside the grooves.

2. Design of the corrugated metallic metasurface absorber

Our Otto geometry [22] based metasurfaces absorber is composed of the PE prism (with apex angle $\beta = 120^\circ$, refractive index of $n_p = 1.54$, and internal incident angle $\theta_{in} = 64^\circ$) and the SPS consisting of 1D array of subwavelength trapezoidal grooves with period p , depth h , top width w_t , and bottom width w_b , as shown in Fig. 1. The processing of the corrugated metallic metasurface is divided into two steps. Firstly, a 500 μm thick silicon wafer (36 mm \times 20 mm) decorated with trapezoidal trench profile array is obtained through deep reactive ion etching (DRIE). Secondly, a 600 nm thick gold layer is sputtered onto the processed silicon wafer to form the SPS, as represented in Fig. 1. Details of the metasurfaces fabrication are described in Methods. Since the gold layer is much thicker than its skin depth at THz the THz regime (approximately 80 nm at 1 THz), the final metallic surface closely resembles a decorated perfect electrical conductor surface. It is held parallel to the PE prism underside and attached to a high precision translation stage which drives the metasurface to control the gap g between PE prism bottom and metasurface, i.e., the free-spaced layer thickness. Because its typical thickness scale is mainly determined by the decaying length of the evanescent field, which is approximately equal to the wavelength of the incident wave (300 μm at 1 THz) [23,24]. Thus, it can be exactly controlled by high precise translation stage. This MPAs with attenuated total reflection (ATR) [25] structure are designed to achieve perfect absorption via minimizing the reflectivity through coupling prism to fulfill the momentum matching between the incident TM-polarized THz waves and the highly-confined

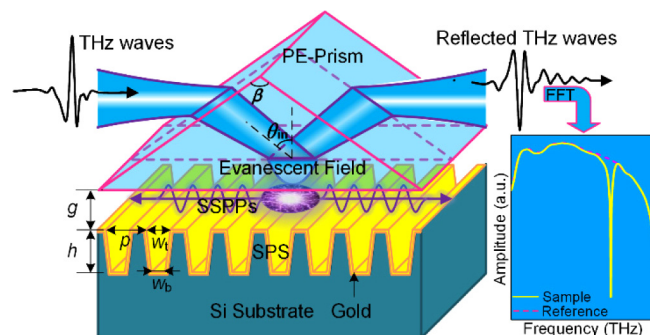


Fig. 1. Schematic of THz-MPA with Otto geometry. Through ATR at the base of PE prism, part of the THz wave will couple into SSPPs wave traveling along the SPS, thus forming an absorbing dip in the reflected THz spectrum.

spoof surface plasmon polaritons (SSPPs) modes, i.e.,

$$k_{\text{SSPPs}} = k_{\parallel} = k_0 n_p \sin \theta_{in}, \quad (1)$$

where $k_0 = 2\pi f/c$, is the vacuum wavevector, k_{\parallel} is the parallel component of wavevector of the incident wave in the PE prism, and k_{SSPPs} is the parallel components of SSPPs modes. Through the excitation of an evanescent field created by the total internal reflection of THz radiation, part of the THz wave will couple into SSPPs wave traveling along the SPS, thus forming an absorbing dip in the reflected THz spectrum.

3. Results and discussions

Figure 2(a) shows optical microscope images of four fabricated SPS samples (I, II, III, and IV with period $p = 60 \mu\text{m}$) with top widths w_t of 32, 31, 31, and 45 μm , bottom widths w_b of 21, 20, 21, and 27 μm , and depths h of 30, 60, 90, and 90 μm (Note that the groove depths of the fabricated SPSs were measured with a film-thickness meter due to their larger depths). We have studied the SSPPs propagation on four planar gold surfaces decorated with linear array of trapezoidal grooves in the Brillouin zone. Figure 2(b) shows the dispersion relation (scatter plots) for the four samples by FEM calculation with COMSOL Multiphysics software. As a comparison, we also plot the dispersion curves of SPSs consisting of periodic square grooves with w_{eff} , i.e., $w_{\text{eff}} = w_t = w_b$, using an effective medium approximation model [26]:

$$k_{\text{SSPPs}} = (\epsilon_d k_0^2 + ((w_{\text{eff}} \epsilon_d) / (p \epsilon_g))^2 k_g^2 \tan^2(k_g h))^{1/2}, \quad (2)$$

where, $k_g = k_0 \sqrt{\epsilon_g} (1 + l_s(i+1)/w_{\text{eff}})^{1/2}$, $l_s = (k_0 \text{Re} \sqrt{-\epsilon_m})^{-1}$, is the skin depth of gold, ϵ_d is the permittivity of the material attached to the corrugated surfaces, ϵ_g is the permittivity of the medium inside the grooves, and ϵ_m is the complex permittivity of gold. Note that all these SSPPs modes plotted in Fig. 2(b) are the fundamental modes. As seen from Fig. 2(b), the scatter data for our fabricated metasurfaces mainly fall into the area enclosed by two dispersion relation curves of square grooves with $w_{\text{eff}} = w_t$ and $w_{\text{eff}} = w_b$. This means that the properties of the SSPPs modes supported on the trapezoidal grooves resemble that of square grooves. Specifically, it is tend to the curve of $w_{\text{eff}} = w_b$. The reason is that the electric field distribution of the trapezoidal groove permeates gradually from the groove top to the groove inside as groove depth increases (as shown in the inset of Fig. 2(b)). Furthermore, it deviate from the light line but intersect with the line of parallel wavevector k_{\parallel} . The intersection point (i.e., momentum matching point) determine the resonance frequency, at which the incident THz wave will couple into SSPPs wave. In addition, the deeper the groove depth, the lower resonance frequency. The same is true for the groove width. But compared with the groove depth, the groove width has a less effect on modulation of the resonant frequency. This suggest that the frequency of the trapping wave can be tailored by properly designing the groove depth. Compared to the previous absorbers, the corrugated metasurface-based absorber presents great advantage for the resonance frequency modulation due to its simple 1D geometric structure.

We utilize a photo-conductive terahertz time-domain spectrometer (THz-TDS) system which filled with nitrogen gas to measure the electromagnetic response of the designed absorber to the free-space layer thickness g . Figure 3(a) shows experimental time-domain signals of the MPA with sample III at varying g (Note that only three representative sets of time-domain signals are plotted and shifted for visual clarity). The reference signal are obtained in the absence of the SPS beneath the prism. As it can be seen, a pronounced ringing has been gradually formed with the decreases of gap, but it will slows down and reduce the spectrum as the gap further decreases. To get a better view of the electromagnetic responses, the measured absorption spectra are plotted in Fig. 3(b). Due to the internal total reflection of the prism, the absorptivity can be calculated by

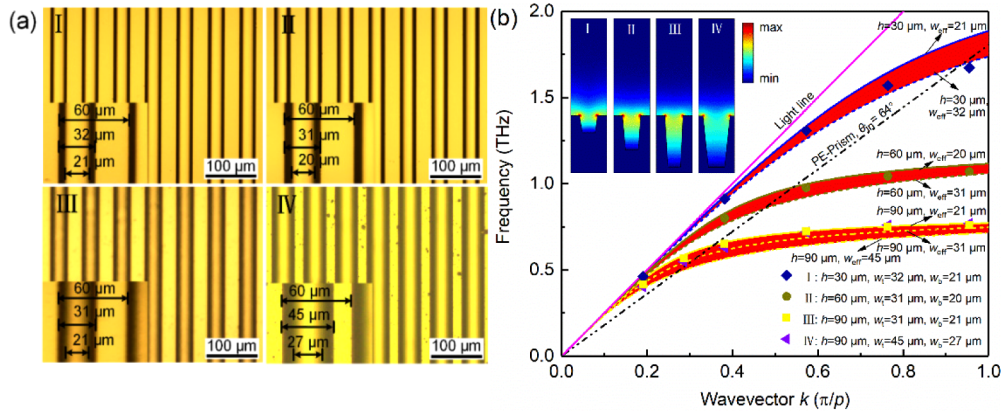


Fig. 2. (a) Optical microscopy images of four corrugated SPS samples with different sizes of trapezoidal groove unit. (b) SSPPs dispersion relation (diamond, roundness, rectangle, and triangle) for sample I, II, III, and IV by FEM calculation with COMSOL software in the Brillouin zone. The curves are the calculation results of SPSs decorated with square grooves using an effective medium approximation model. The pink and black double dots curves indicate the light line and the parallel wavevector k_{\parallel} , respectively. The insets show the electric field distributions for the unit cell of the four SPS samples near the Brillouin zone.

the formula:

$$A(\omega) = 1 - R(\omega), \quad (3)$$

Where $R(\omega) = |E(\omega, g)/E(\omega, g \rightarrow \infty)|^2$, is the reflectivity. As is apparent, the absorption spectrum broadens and red-shifts with the decrease of gap, including the resonance frequency f_{sp} changes from 0.655 THz for $g = 250 \mu\text{m}$ to 0.557 THz for $g = 130 \mu\text{m}$. This is because a portion of the SSPPs field will outcoupling into the prism result in an additional damping of SSPPs at narrower gap [27,28]. Meanwhile, the absorption coefficient appears change that increases first but then drops. In particular, there exists an optimal free-space layer thickness that enables the complete destructive interference of the reflected light and thereby gaining perfect absorption at a specific frequency. A peak absorption of $A = 99.97\%$ with $f_{sp} = 0.625 \text{ THz}$ at $g = 190 \mu\text{m}$ can be observed from the measured absorption spectra. Except for the appearance of characteristic absorption peak, another key feature of SPR is the abrupt phase jump near the resonance frequency. The phase change is defined as the difference in phase of each frequency component of the sample ϕ_{sam} and reference ϕ_{ref} spectra, i.e.,

$$\Delta\phi = \phi_{sam} - \phi_{ref}. \quad (4)$$

As shown in Fig. 3(c), the phase change spectrum has a region with a sharp jump near the absorption peak. Interestingly, the direction of phase jump transits from positive to negative when the gap reduce to $180 \mu\text{m}$. And it does that because of the modulation of the optimal resonance condition (i.e., R passes through the point $R = 0$) caused by the tiny change of coupling gap [29]. Thus, the direction change of phase jump further proves that perfect absorption can be achieved via properly adjusting the thickness of the free-space layer.

Figure 4 shows experimental absorption spectra 4(a) and phase change spectra 4(b) of the MPAs with SPS samples of different depths and widths (I, II, III, and IV, as shown in Fig. 2(a)) at their respective relatively optimal coupling gaps ($g = 75, 130, 190,$ and $215 \mu\text{m}$). As it can be seen, all absorption spectra exhibit near perfect absorption along with a sharp phase jump. The absorption values we acquired for the four SPS samples are 99.99%, 99.52%, 99.97%, and 99.50%, respectively. These experimental results are a good validation of the previous inference

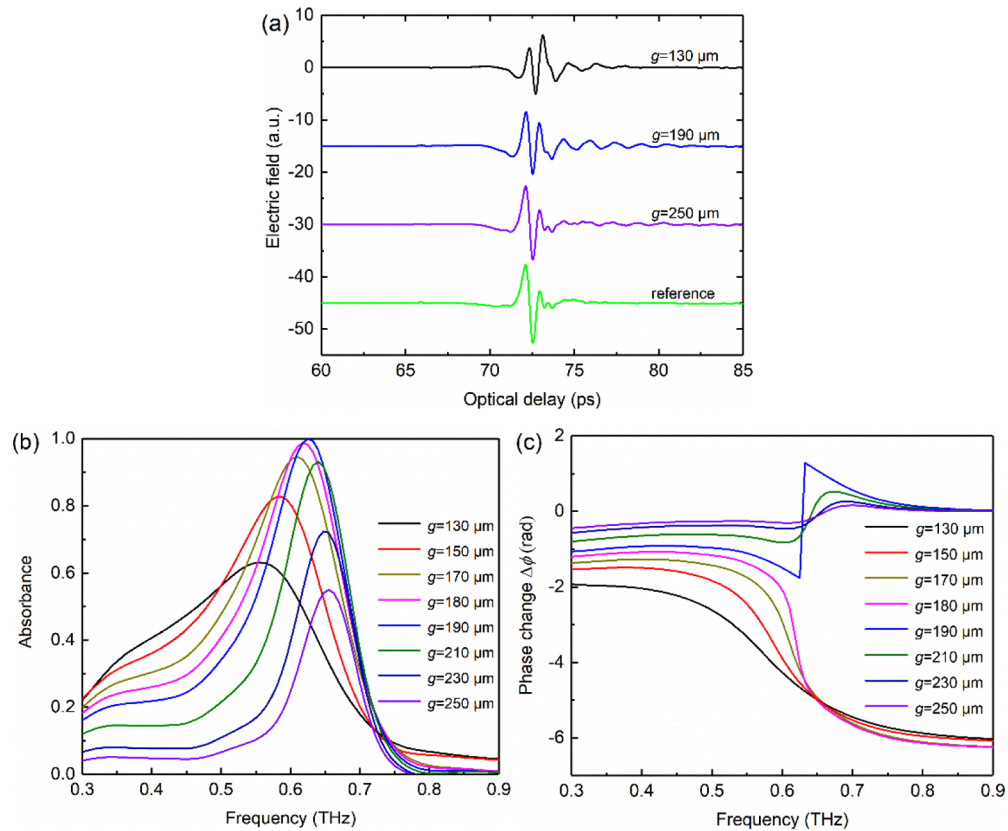


Fig. 3. Experimental time-domain signals (a), absorption spectra (b), and phase change spectra (c) of the MPA with sample III at varying free-space coupling gaps g . The measured time-domain signals are shifted for visual clarity.

that perfect absorption can be acquired by properly modulating the thickness of the coupling layer. Meanwhile, their resonance frequencies agree well with the theoretical predictions by the SSPPs dispersion relation (as shown in the Fig. 2(b)). Specifically, we can see a dramatic red-shift in the absorption peaks as the groove depth increases, which reduces from 1.499 THz for $h = 30\ \mu\text{m}$ to 0.625 THz for $h = 90\ \mu\text{m}$. The emergence of the absorption frequency shifts is attributed to the lower asymptotic frequency of SSPPs dispersion relation. Previous theoretical studies have showed that the high-order SSPPs mode with the order of m can be supported, when h is large enough, i.e., $h > mp$ (integer m is the order of the mode) [24]. But higher order SSPPs usually excited with a narrower coupling gap due to their higher asymptotic frequency, increasing the difficulties of the excitation of SSPPs and the controlling of the absorption by the central layer of the absorber. Also, the experimental results of sample III and IV (which shifts from 0.625 THz for $w_t = 30\ \mu\text{m}$ to 0.550 THz for $w_t = 45\ \mu\text{m}$) verify our theoretical analysis that a small red-shift of resonance frequency occurs with the groove width increases. But the modulation length of groove width is very limited by the groove period. For comparison, their corresponding absorption and phase change were calculated via 2D numerical simulation by COMSOL Multiphysics software. The inset of Fig. 4(c) shows the unit cell of the 2D simulation model. A periodic boundary condition was applied along the direction of periodicity to simulate a linear array of trapezoidal grooves. Besides, the gold film was simulated using a transition boundary condition at the grooves surface; the permittivity of gold at THz frequencies is described by the Drude model

with plasma frequency $\omega_p = 1.367 \times 10^{16}$ rad/s and scattering frequency $\gamma_p = 4.072 \times 10^{13}$ rad/s (Ref. [30]). As seen from Fig. 4(c) and 4(d), the variation trend of the simulated absorption spectra and phase change spectra with different depths and widths are in agreement with the measurements. The main difference between the calculations and experiments lies in the full width at half maximum (FWHM) of the absorption spectra. The primary reasons are the increase in absorption losses caused by the formation of hot spots at the structural imperfections in the SPS samples and diffraction effects resulting from the scattering of the SSPPs modes at the edges of the SPS. Meanwhile, the structural imperfections of SPS samples also lead to the small shift of the optimal resonance frequency. The frequency modulation response of the simple 1D resonator structure demonstrates that such MPA has a significant design flexibility that the resonance frequency can be precisely adjusted by the groove depth.

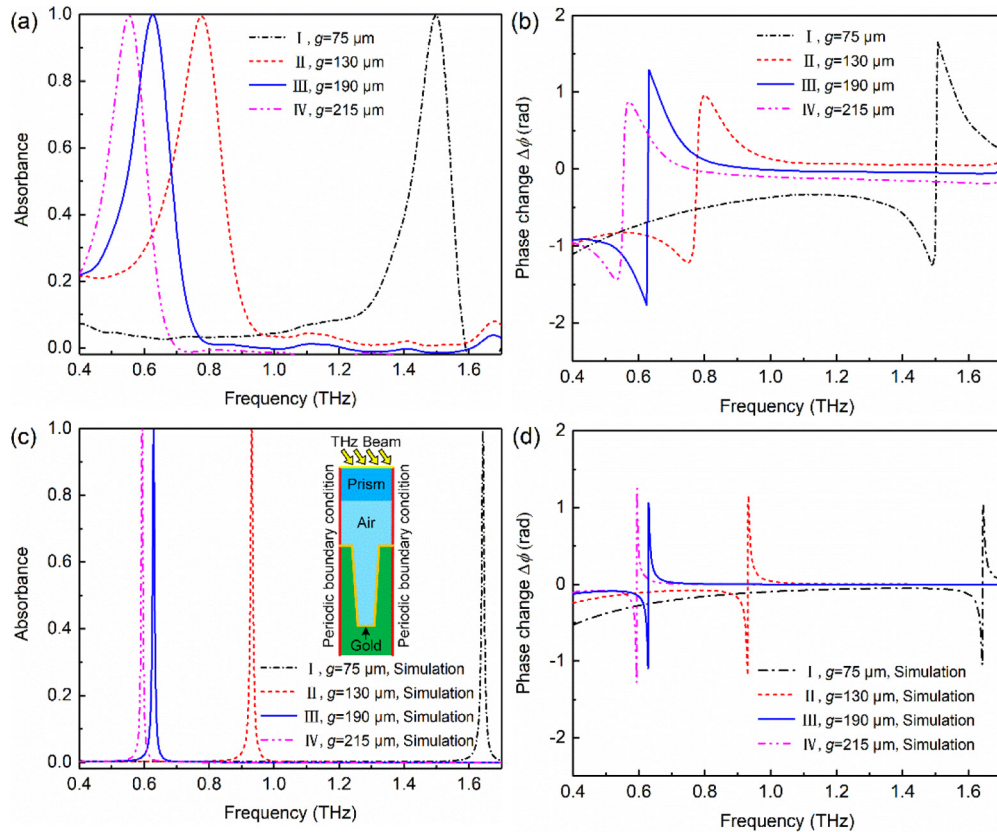


Fig. 4. Experimental absorption spectra (a), and phase change spectra (b) of the MPA with SPS samples of different depths and widths (I, II, III, and IV) at their respective relatively optimal coupling gaps g . The corresponding simulated absorption spectra (c), and phase change spectra (d). The inset shows the unit cell of the 2D simulation model.

We have also investigated the absorption response of the MPA in different dielectric environment. Figure 5 shows the experimental absorption spectra 5(a) and phase change spectra 5(b) of the MPA with sample I in which its grooves filled with water. As it can be seen, there appear a similar perfect absorption peak with a bandwidth of about 0.35 THz and an absorptivity of more than 90%, instead of the complete attenuation of terahertz signal. Compared with that of air, the absorption peak broadens and red shifts markedly as water filling the grooves. This is due to the increase of the effective refractive index and loss of dielectric environment with

the addition of water. At the same time, we also can observe a similar phase jump in a wider frequency range, which proves again the excitation of SSPPs mode, as shown in Fig. 5(b). Thus, the effective refractive index and loss modulation can be accepted as an alternative approach for the absorption properties modulation. This design method is also useful for the design of metasurface modulators in other frequency band such as microwave region [31]. In addition, it is important to note that the conventional MPAs with direct irradiation modes, reaches its limit when applied to discern analytes dissolved in polar liquids due to their extremely high absorption in THz regime [32]. But this new MPAs combined with ATR technique provides a potential route to overcome the limitation due to the shorter interaction length of evanescent wave [33], which is particularly important for biological sensing [34,35].

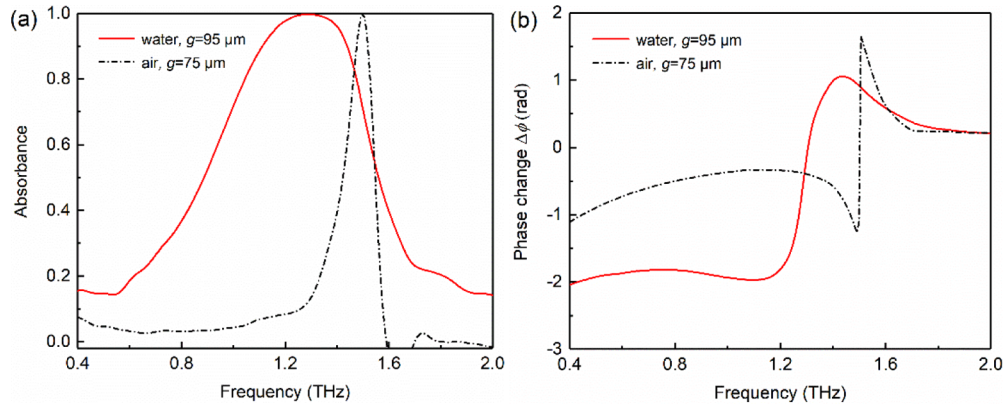


Fig. 5. Experimental absorption spectra (a), and phase change spectra (b) of the MPAs with sample I in which its grooves filled with water and air.

4. Conclusions

In this letter, we have experimentally realized a perfect metasurface absorber with ATR structure. It has been demonstrated that a continuous evolution of absorption resonances occurs with the decreasing free-space layer thickness, which provides a feasible approach to tune the absorption. Specifically, the direction of phase jump will change under a certain coupling gap, which indicates that the perfect absorption (i.e., $A = 100\%$) can be achieved by properly modulating the coupling gap. Experiments indicate that all our four samples resulted in almost perfect absorption effect, with absorption efficiency at 99.99%, 99.52%, 99.97% and 99.50% respectively. Moreover, we also demonstrated that the near perfect absorption can be acquired over a wide frequency range (0.625–1.499 THz) just by modulating the depth of the groove. These experimental results confirmed that the asymptotic frequency of SPSs dispersion relation is quite sensitive to the groove depth. The emerging of 1D corrugated metasurfaces solves the problems of frequency modulation of most MPAs with complicated geometries. More importantly, similar results can be achieved by changing the refractive index and loss inside the grooves, benefit from the high sensitivity of SSPPs wave to the dielectric environment. Besides, our experimental results also inform that the strong absorption of electromagnetic field energy by polar liquid can be alleviate effectively by prism coupling. This means that MPA can be utilized as a good platform for THz-SPR sensing, especially in biological sensing.

5. Methods

SPSs consisting of a periodic trapezoidal groove array were fabricated via conventional deep reactive ion etching (DRIE) on 500 μm thick silicon wafers. Before the DRIE process, a thick

layer of AZ 5214E positive photoresist was coated onto the Si substrate via spin coating process. The AZ 5214E was spun at 2000 rpm for 30 s followed by a soft bake at 100 °C for 60 s, giving a final photoresist thickness of approximately 2 μm. Then, the photoresist is exposed to UV light via a pre-fabricated photomask in a mask aligner (Karl Suss, MA6/BA6) with a dosage of 1000 mJ/cm² and developed with AZ 400K developer to reveal the etched mask of groove array. After that, the DRIE using Bosch process was performed in deep silicon etching equipment (Alcatel) with an radio frequency of 13.56 MHz, a chamber pressure of 10 mTorr, and a gas flow rate of 450 sccm to give a silicon groove array with varying depths and an overall area of 20 mm × 35 mm. Finally, 600 nm of gold is sputtered onto the silicon groove array (Explorer-14) to give the final SPS.

Funding

National Natural Science Foundation of China (51675103); Fujian Provincial Science and Technology Project (2019I0004); State Key Laboratory of Mechanical System and Vibration (MSV-2018-07); Shanghai Natural Science Fund (18ZR1414200).

Acknowledgments

Thanks for the discussions with Dr. Gaofeng Zheng of Xiamen University, China.

References

1. H. Inoue, K. Kawase, Y. Ogawa, and Y. Watanabe, "Non-destructive terahertz imaging of illicit drugs using spectral fingerprints," *Opt. Express* **11**(20), 2549–2554 (2003).
2. J. M. Jornet and I. F. Akyildiz, "Femtosecond-long pulse-based modulation for terahertz band communication in nanonetworks," *IEEE Trans. Commun.* **62**(5), 1742–1754 (2014).
3. J. Liu, J. Dai, S. L. Chin, and X. C. Zhang, "Broadband terahertz wave remote sensing using coherent manipulation of fluorescence from asymmetrically ionized gases," *Nat. Photonics* **4**(9), 627–631 (2010).
4. S. Zhong, "Progress in terahertz nondestructive testing: A review," *Front. Mech. Eng.* **14**(3), 273–281 (2019).
5. W. Withayachumnankul, G. M. Png, X. Yin, S. Atakaramians, I. Jones, H. Lin, B. S. Y. Ung, J. Balakrishnan, B. W.-H. Ng, B. M. Fischer, D. Abbott, B. Ferguson, and S. P. Micken, "T-ray sensing and imaging," *Proc. IEEE* **95**(8), 1528–1558 (2007).
6. G. Markelz, A. Roitberg, and E. J. Heilweil, "Pulsed terahertz spectroscopy of DNA, bovine serum albumin and collagen between 0.1 and 2.0 THz," *Chem. Phys. Lett.* **320**(1–2), 42–48 (2000).
7. P. K. Sahoo, K. Vogelsang, H. Schiff, and H. H. Solak, "Surface plasmon resonance in near-field coupled gold cylinder arrays fabricated by euv-interference lithography and hot embossing," *Appl. Surf. Sci.* **256**(2), 431–434 (2009).
8. A. Ahmadiwand, R. Sinha, B. Gerislioglu, M. Karabiyik, N. Pala, and M. Shur, "Transition from capacitive coupling to direct charge transfer in asymmetric terahertz plasmonic assemblies," *Opt. Lett.* **41**(22), 5333–5336 (2016).
9. M. Qiu, M. Jia, S. Ma, S. Sun, Q. He, and L. Zhou, "Angular Dispersions in Terahertz Metasurfaces: Physics and Applications," *Phys. Rev. Appl.* **9**(5), 054050 (2018).
10. R. Singh, W. Cao, I. Al-Naib, and L. Cong, "Ultrasensitive terahertz sensing with high-Q fano resonances in metasurfaces," *Appl. Phys. Lett.* **105**(17), 171101 (2014).
11. C. M. Watts, D. Shrekenhamer, J. Montoya, G. Lipworth, J. Hunt, T. Sleasman, S. Krishna, D. R. Smith, and W. J. Padilla, "Terahertz compressive imaging with metamaterial spatial light modulators," *Nat. Photonics* **8**(8), 605–609 (2014).
12. A. Ahmadiwand, B. Gerislioglu, A. Tomitaka, P. Manickam, A. Kaushik, S. Bhansali, M. Nair, and N. Pala, "Extreme sensitive metasensor for targeted biomarkers identification using colloidal nanoparticles-integrated plasmonic unit cells," *Biomed. Opt. Express* **9**(2), 373–386 (2018).
13. N. I. Landy, S. Sajuyigbe, J. J. Mock, D. R. Smith, and W. J. Padilla, "Perfect metamaterial absorber," *Phys. Rev. Lett.* **100**(20), 207402 (2008).
14. A. A. Basharin, V. Chuguevsky, N. Volsky, M. Kafesaki, and E. N. Economou, "Extremely high Q-factor metamaterials due to anapole excitation," *Phys. Rev. B* **95**(3), 035104 (2017).
15. J. Zhu, Z. Ma, W. Sun, F. Ding, Q. He, L. Zhou, and Y. Ma, "Ultra-broadband terahertz metamaterial absorber," *Appl. Phys. Lett.* **105**(2), 021102 (2014).
16. X. Y. Peng, B. Wang, S. Lai, D. H. Zhang, and J. H. Teng, "Ultrathin multi-band planar metamaterial absorber based on standing wave resonances," *Opt. Express* **20**(25), 27756–27765 (2012).
17. D. Lim, D. Lee, and S. Lim, "Angle- and polarization-insensitive metamaterial absorber using via array," *Sci. Rep.* **6**(1), 39686 (2016).

18. Y. Ma, Q. Chen, J. Grant, S. C. Saha, A. Khalid, and D. R. Cumming, "A terahertz polarization insensitive dual band metamaterial absorber," *Opt. Lett.* **36**(6), 945–947 (2011).
19. G. Yao, F. Ling, J. Yue, C. Luo, J. Ji, and J. Yao, "Dual-band tunable perfect metamaterial absorber in the THz range," *Opt. Express* **24**(2), 1518–1527 (2016).
20. G. Yuan, J. Schalch, X. Zhao, J. Zhang, R. D. Averitt, and X. Zhang, "Analysis of the thickness dependence of metamaterial absorbers at terahertz frequencies," *Opt. Express* **26**(3), 2242–2251 (2018).
21. S. Jacob, G. Duan, X. Zhao, X. Zhang, and R. D. Averitt, "Terahertz metamaterial perfect absorber with continuously tunable air spacer layer," *Appl. Phys. Lett.* **113**(6), 061113 (2018).
22. A. Otto, "Excitation of nonradiative surface plasma waves in silver by the method of frustrated total reflection," *Z. Phys. A: Hadrons Nucl.* **216**(4), 398–410 (1968).
23. H. Hirori, M. Nagai, and K. Tanaka, "Destructive interference effect on surface plasmon resonance in terahertz attenuated total reflection," *Opt. Express* **13**(26), 10801–10814 (2005).
24. H. Yao and S. Zhong, "High-mode spoof spp of periodic metal grooves for ultra-sensitive terahertz sensing," *Opt. Express* **22**(21), 25149–25160 (2014).
25. H. Hirori, K. Yamashita, M. Nagai, and K. Tanaka, "Attenuated total reflection spectroscopy in time domain using terahertz coherent pulses," *Jpn. J. Appl. Phys.* **43**(10A), L1287–L1289 (2004).
26. A. Rusina, M. Durach, and M. I. Stockman, "Theory of spoof plasmons in real metals," *Appl. Phys. A: Mater. Sci. Process.* **100**(2), 375–378 (2010).
27. C. H. Gan, "Analysis of surface plasmon excitation at terahertz frequencies with highly doped graphene sheets via attenuated total reflection," *Appl. Phys. Lett.* **101**(11), 111609 (2012).
28. Y. Huang, S. Zhong, H. Yao, and D. Cui, "Tunable Terahertz Plasmonic Sensor Based on Graphene/Insulator Stacks," *IEEE Photonics J.* **9**(1), 1–10 (2017).
29. Y. Huang, S. Zhong, Y. Shen, Y. Yu, and D. Cui, "Terahertz phase jumps for ultra-sensitive graphene plasmon sensing," *Nanoscale* **10**(47), 22466–22473 (2018).
30. M. A. Ordal, L. L. Long, R. J. Bell, S. E. Bell, R. R. Bell, R. W. Alexander Jr., and C. A. Ward, "Optical properties of the metals Al, Co, Cu, Au, Fe, Pb, Ni, Pd, Pt, Ag, Ti, and W in the infrared and far infrared," *Appl. Opt.* **22**(7), 1099–1120 (1983).
31. Y. Yuan, K. Zhang, X. Ding, B. Ratni, S. N. Burokur, and Q. Wu, "Complementary transmissive ultra-thin meta-deflectors for broadband polarization-independent refractions in the microwave region," *Photonics Res.* **7**(1), 80–88 (2019).
32. M. Heyden and M. Havenith, "Combining THz spectroscopy and MD simulations to study protein-hydration coupling," *Methods* **52**(1), 74–83 (2010).
33. Y. Zou, Q. Liu, X. Yang, H. Huang, J. Li, L. Du, Z. Li, J. Zhao, and L. Zhu, "Label-free monitoring of cell death induced by oxidative stress in living human cells using terahertz ATR spectroscopy," *Biomed. Opt. Express* **9**(1), 14–24 (2018).
34. X. Wu, B. Quan, X. Pan, X. Xu, X. Lu, C. Gu, and L. Wang, "Alkanethiol-functionalized terahertz metamaterial as label-free, highly-sensitive and specific biosensor," *Biosens. Bioelectron.* **42**, 626–631 (2013).
35. D. Lee, J. Kang, J. Kwon, J. Lee, S. Lee, D. H. Woo, J. H. Kim, C. Song, Q. Park, and M. Seo, "Nano metamaterials for ultrasensitive Terahertz biosensing," *Sci. Rep.* **7**(1), 8146 (2017).